

The High field magnetization of FePS 3

A. R Wildes, D. Lançon, M. K Chan, F. Weickert, N. Harrison, V. Simonet, M. E. Zhitomirsky, M. V Gvozdikova, T. Ziman, H. M Rønnow

▶ **To cite this version:**

A. R Wildes, D. Lançon, M. K Chan, F. Weickert, N. Harrison, et al.. The High field magnetization of FePS 3. Physical Review B, 2020, 101 (2), pp.024415. 10.1103/PhysRevB.101.024415 . hal-03029896

HAL Id: hal-03029896
https://cnrs.hal.science/hal-03029896

Submitted on 29 Nov 2020

HAL is a multi-disciplinary open access archive for the deposit and dissemination of scientific research documents, whether they are published or not. The documents may come from teaching and research institutions in France or abroad, or from public or private research centers.

L'archive ouverte pluridisciplinaire **HAL**, est destinée au dépôt et à la diffusion de documents scientifiques de niveau recherche, publiés ou non, émanant des établissements d'enseignement et de recherche français ou étrangers, des laboratoires publics ou privés.

The high field magnetisation of $FePS_3$

A. R. Wildes*
Institut Laue-Langevin, 71 avenue des Martyrs CS 20156, 38042 Grenoble Cedex 9, France

D. Lançon†
Institut Laue-Langevin, 71 avenue des Martyrs CS 20156, 38042 Grenoble Cedex 9, France and Ecole Polytechnique Fédérale de Lausanne, SB ICMP LQM, CH-1015 Lausanne, Switzerland

M. K. Chan
Los Alamos National Laboratory, Los Alamos, NM 87545, USA

F. Weickert
NHMFL, Florida State University, Tallahassee FL, 32310, USA

N. Harrison
Los Alamos National Laboratory, Los Alamos, NM 87545, USA

V. Simonet
Institut Néel, CNRS & Univ. Grenoble Alpes, 38042 Grenoble, France

M. E. Zhitomirsky
Univ. Grenoble Alpes, CEA, IRIG, PHELIQS, 17 avenue des Martyrs, 38000 Grenoble, France

M. V. Gvozdikova
Institut Laue-Langevin, 71 avenue des Martyrs CS 20156, 38042 Grenoble Cedex 9, France

T. Ziman
Institut Laue-Langevin, 71 avenue des Martyrs CS 20156, 38042 Grenoble Cedex 9, France and Univ. Grenoble Alpes, CNRS, LPMMC, 38000 Grenoble, France

H. M. Rønnow
Ecole Polytechnique Fédérale de Lausanne, SB ICMP LQM, CH-1015 Lausanne, Switzerland

(Dated: January 15, 2020)

High field magnetisation measurements in pulsed fields up to 65 Tesla have been performed on $FePS_3$, which is nominally a good example of a two-dimensional Ising-like antiferromagnet on a honeycomb lattice. Measurements with the field parallel to the moment direction confirm the presence of two first-order transitions above 35 Tesla, to $M/M_{sat} = 1/2$ and $M/M_{sat} = 1$, respectively, at 4 K. The measurements are in contradiction with published estimates for the magnetic exchange parameters, but the contradiction can be resolved by allowing for anisotropic exchange parameters in the Hamiltonian. The magnetisation with the field perpendicular to the moment direction is anisotropic, with no transitions observed for fields along the **a** axis while a cascade of first-order transitions is observed for fields above 50 Tesla along the **b** axis, the latter case also showing a strong degradation of the sample after repeated pulses. The results indicate a strong magneto-lattice coupling in $FePS_3$. Temperature-dependent measurements hint at a possible tricritical point.

I. INTRODUCTION

$FePS_3$ belongs to a family of quasi-two dimensional layered compounds [1]. The compounds are isostructural, all having the monoclinic space group $C\frac{2}{m}$ with the *ab* planes forming the layers that are stacked along the **c** axis [2]. The *ab* planes are weakly bound by van der Waals forces, with the iron atoms forming a honeycomb lattice within the layer plane. The compounds have attracted considerable attention over the years due to their layered structure. They can be intercalated with guest atoms and molecules including lithium, and hence were considered to be candidates for battery materials [1, 3]. The compounds can be delaminated to monolayer thickness. This has attracted the interest of the graphene community as, unlike graphene, the compounds are also magnetic [4–6] and $FePS_3$ maintains its magnetic characteristics down to a monolayer [7].

The weak coupling between the layers is such that,

* wildes@ill.fr
† Current address: Paul Scherrer Institute, WHGA/150, 5232 Villigen PSI, Switzerland

even in bulk form, the compounds are good examples of model magnets in two dimensions and hence they are important compounds for testing theories of magnetism. $FePS_3$ is of special interest as it appears to be a good example of a two-dimensional Ising antiferromagnet, ordering below a Néel temperature of ~ 120 K. The phase transition is thought to be of first order due to a discontinuous change in the variation of the lattice parameters with temperature [8, 9]. Its ordered magnetic structure is shown in figure 1(a) [1, 10, 11]. The structure consists of ferromagnetic 'zig-zag' chains that run parallel to the **a** axis. The chains are antiferromagnetically coupled along the **b** axis. The moments point along the $\mathbf{c}^*$ direction, which is normal to the *ab* planes. The moments are antiferromagnetically coupled between the planes due a weak interlayer magnetic exchange, estimated from neutron spectroscopy to be $\sim 1/200$ the magnitude of the nearest-neighbour exchange [11]. The temperature-dependence of the sublattice magnetisation is consistent with that expected for an Ising model [12].

The Ising-like behaviour is due to strong anisotropy, as observed by Mössbauer spectroscopy [8], magnetic susceptibility [8, 14], and in the appearance of a large gap in the spin waves at the Brillouin zone centre [11]. The compound is not fully Ising-like as, in its ordered state, it has dispersive magnons [11]. However, $FePS_3$ may be close enough to being a model Ising magnet to test a number of intriguing theories.

High-field magnetisation experiments of Ising systems, particularly for a transverse field, are of particular interest. The model has been extensively studied theoretically and, despite its simplicity, can result in fascinating behaviour such as quantum phase transitions and tricritical points [15–18]. Such experiments on $FePS_3$ would determine whether the compound is a satisfactory physical representation to test the theories.

High-field magnetisation measurements have previously been performed in $FePS_3$. Okuda *et al.* performed magnetisation measurements in a pulsed magnetic field up to 40 Tesla [19] with the field applied parallel to the moment direction, i.e. parallel to the $\mathbf{c}^*$ axis. The magnetisation showed two abrupt transitions as the field was increased at 4.2 K: a transition to half the saturation magnetisation, $M_{sat}/2$, occurred at ~ 38 Tesla followed by a transition to M_{sat} at ~ 40 Tesla. The magnetisation showed hysteresis, with the two transitions occurring at lower fields as the pulsed field decreased. The two transitions decreased in field with increasing temperature, eventually becoming a single transition with a much more continuous change of magnetisation with field at ~ 100 K.

Okuda *et al.* used the critical fields for the two transitions at 4.2 K with the measured Curie-Weiss temperature to estimate the magnetic exchange interactions using a classical mean-field model. They also estimated the magnitude of a single-ion anisotropy, Δ, from a paramagnetic resonance study. More recently, Lançon *et al.* have performed neutron spectroscopy to measure the spin waves in $FePS_3$, using linear spin wave theory to derive the exchange and anisotropy parameters from the dispersion [11]. Both sets of data were modelled using the same Hamiltonian:

$$\hat{\mathcal{H}} = -\sum_{\langle ij \rangle} J_{ij} \mathbf{S}_i \cdot \mathbf{S}_j - \Delta \sum_i \left(S_i^z\right)^2 - H^z \sum_i S_i^z, \quad (1)$$

where the ordered moment direction is along z and, for simplicity, the applied field H is given in units of $g\mu_B$ where g is the spectroscopic splitting factor and μ_B is the Bohr magneton. J_{ij} is the exchange between two moments, S_i and S_j, and it may be expressed in terms of the exchange between neighbours at various distances. Examples of the exchange interactions between first, second and third nearest neighbours in the (ab) planes are shown in Figure 1(b), labelled J_1, J_2 and J_3 respectively. The very weak interplanar exchange will be ignored in the following discussion. No external field was used for the neutron spectroscopy measurements, i.e. $H^z = 0$ in the analysis of these data.

The parameters determined from both studies are listed in Table I. Inspection of the table shows that the values for Δ and the nearest-neighbour exchange J_1 compare reasonably well. However, the values for J_2 and J_3, the second and third nearest-neighbour exchanges respectively, differ substantially.

The discrepancies between the two sets of parameters reflect a contradiction between the high-field magnetisation and neutron spectroscopy data. The parameters from the analysis by Okuda *et al.* give rise to the observed two transitions in the high-field magnetisation, but do not reproduce the spin wave dispersion. The parameters from Lançon *et al.*, by definition, reproduce the measured spin wave dispersion. However, according to the analysis by Okuda they will not give a transition to $M_{sat}/2$ in the high-field magnetisation.

This article reports a study of the high-field magnetisation $FePS_3$. Experimental data with fields up to 65 Tesla are presented. The fields were applied along four high-symmetry directions: along the $\mathbf{c}^*$ to verify the measurements by Okuda *et al* and to attempt to resolve the discrepancy between the two sets of exchange parameters shown in Table I; and along three different directions with $\mathbf{H} \perp \mathbf{c}^*$ to search for exotic effects predicted by theory. The article is divided into the following sections:

Section II contains a summary of the relevant theory for high-field magnetisation in Ising-like models. The section includes an updated calculation for the stability phase diagram for an Ising model on a honeycomb lattice in a field applied along z, revealing further discrepancies with the parameters given in Table I. Section III contains a description of the sample preparation and experimental methods used in the study. The experimental data are given in Section IV. The data from Okuda *et al.* are verified for measurements with $\mathbf{H} \parallel \mathbf{c}^*$, however the experiments revealed a number of surprising results including a dependence on whether the sample was in a liquid or gaseous helium environment, and a

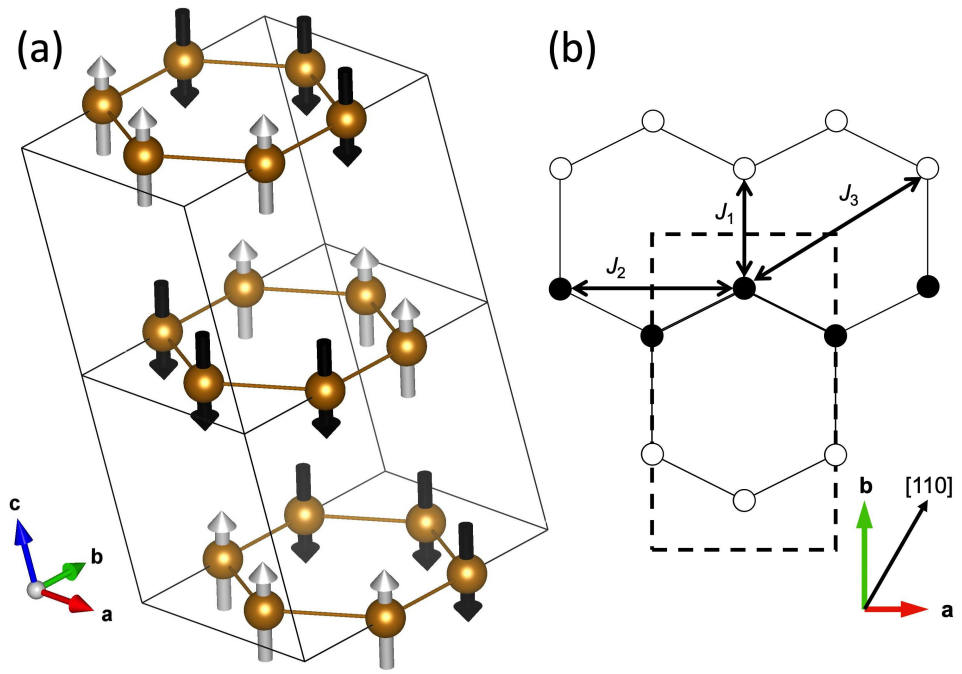


FIG. 1. (a) The magnetic structure of $FePS_3$ in zero field, showing the magnetic moments on the Fe^{2+} ions . The moments point normal to the *ab* planes. The figure was created using the VESTA program [13]. (b) The magnetic structure in the *ab* plane, with examples of the exchange interactions between first, second, and third nearest neighbours being labelled with J_1, J_2 and J_3 respectively.

TABLE I. Table showing the best estimates for the exchange parameters and anisotropy in $FePS_3$ from previous high field magnetisation measurements [19] and from neutron spectroscopy [11]. All units are in meV.

	Values from [19]	Values from [11]
J_1	1.69	1.46 (1)
J_2	−0.89	−0.04 (4)
J_3	0.19	−0.96 (5)
Δ	2.95	2.66 (8)

strong anisotropic coupling between the magnetism and the crystal lattice when $\mathbf{H}\perp\mathbf{c}^*$. The results are discussed in section V, where extra anisotropy terms in the Hamiltonian are considered to resolve the discrepancies.

II. THEORY

A. Magnetic structure phase diagram for fields parallel to $\mathbf{c}^*$

The presence of a strong easy-axis anisotropy in equation 1, i.e. $\Delta \gtrsim \max(|J_{ij}|)$, makes the formation of magnetic states with components of the spins perpendicular to z energetically unfavourable. Consequently, the equilibrium states for $\mathbf{H} \parallel z$, corresponding to a field being applied along the $\mathbf{c}^*$ axis of $FePS_3$, may be found by considering a reduced Ising-like Hamiltonian:

$$\hat{\mathcal{H}} = -\sum_{\langle ij \rangle} J_{ij} S_i^z S_j^z - H^z \sum_i S_i^z \ . \qquad (2)$$

The spin model described by Eq. 2 has been investigated by Kudō and Katsura [20], who used an analytical method to find possible classical states of the Ising model on a honeycomb lattice with extended exchange interactions in an applied magnetic field. Their method allows unique ground states to be determined for most parts of the H–J_{ij} space. However, it leaves a region where the stable magnetic structures remain uncertain.

To complement the analytical study by Kudō and Katsura, numerical calculations were performed with the aim to resolve the uncertainties and to provide a complete phase diagram. The calculations consisted of real-space mean-field simulations of the type described by Gvozdikova *et al.* [21]. A cluster of $2 \times 12 \times 12$ sites on a honeycomb lattice with periodic boundary conditions was initiated with a random spin configuration and the moment orientations were allowed to vary to find the stationary state. The procedure was repeated for 10^4 random initial spin configurations and, thus, the absolute minimum was determined for a given value of an applied magnetic field.

The results of the combined analytical and numerical investigation are presented in the phase diagram shown in Figure 2 and and the classical energies of the corresponding states are listed in Table II. The diagram is consistent with that given by Kudō and Katsura. Exchange interactions up to the third nearest-neighbour are included, and the first nearest-neighbour exchange, J_1, is ferromagnetic, i.e. $J_1 > 0$. Five stable structures were found in the absence of a magnetic field for different regimes of the ratios J_2/J_1 and J_3/J_1. Schematics showing the representative structures with their corresponding energies are also shown in the figure. The stability region for the 'zig-zag' structure of $FePS_3$ is in the lower left area of the figure.

The zero-field phase diagram may be compared with a calculation using Equation 1 in the Heisenberg (i.e. $\Delta = 0$) and XY (i.e. $\Delta < 0$) limits [22]. The phase diagrams are similar, with identical collinear structures in roughly the same regions. The Heisenberg and XY models show non-collinear structures in certain regions, which are clearly not allowed for an Ising model. These regions are covered in Figure 2 by extensions of the 'stripe' and 'zig-zag' structures, and by the new 'armchair' structure.

The phase diagram includes the number and magnetisation of phases that become stable as an external magnetic field is applied. The transitions are represented in the diagram as numbers showing the ratio M/M_{sat}. The ferromagnetic state obviously has $M/M_{sat} = 1$ in zero field and has no transition with increasing field. The four antiferromagnetic states have $M/M_{sat} = 0$ in zero field. As the field is increased, the phase diagram becomes further subdivided into regions with first-order phase transitions to magnetic structures with $M/M_{sat} = 1/3$ and $1/2$, where one third and one half of the antiparallel moments will flip to align with the applied field respectively. All parts of the phase diagram will transition to the ferromagnetic structure at sufficiently high fields.

The partially magnetised states are shown in the figure, and their energies are given in Table II. One structure with $M/M_{sat} = 1/3$ is present, while two structures with $M/M_{sat} = 1/2$ appear in different parts of the phase diagram. The structure labelled 1/2(A) was previously suggested by Okuda *et al.* and it appears when a field is applied to a 'zig-zag' structure.

Data points corresponding to the two sets of exchange parameters given in Table I are also shown in Figure 2. Further discrepancies regarding the parameters of Okuda *et al.* are immediately apparent in that they are not consistent with the 'zig-zag' magnetic structure observed for $FePS_3$ in zero field, instead giving the armchair configuration as the stable structure. Furthermore, while these parameters will give a phase transition to an intermediate configuration with increasing field before saturating at a larger field, the intermediate structure has $M/M_{sat} = 1/3$ and not $M/M_{sat} = 1/2$. The exchange parameters of Lançon *et al.* are consistent with the observed magnetic structure for $FePS_3$ in zero field. However, as anticipated from the analysis of Okuda *et al.*, they show only a single transition to $M/M_{sat} = 1$. The region of the phase diagram that would correspond to the measurements of Okuda *et al.* is bound by the inequalities $J_2 \leq -J_1/2$ and $J_3 \leq J_2 + J_1/2$ in the 'zig-zag' zone.

B. Field perpendicular to c*

The Ising model in a transverse field is a well-known quantum theory problem, and some articles have specifically addressed the model with $S = 2$ on a honeycomb lattice [15–18, 23]. These studies have frequently retained a quadratic term in the Hamiltonian to account for crystal field interactions, such that equation 1 becomes:

$$\hat{\mathcal{H}} = -\sum_{\langle ij \rangle} J_{ij} S_i^z S_j^z - \Delta^{cf} \sum_i (S_i^z)^2 - H^x \sum_i S_i^x. \quad (3)$$

The direction of the transverse field, H^x, is defined simply with respect to the direction of the Ising spins. The eigenvalues of the Hamiltonian are therefore independent of the direction of H^x within the crystal lattice plane whose normal is parallel to z.

The exchanges in these studies have largely been confined to being between nearest neighbours. Mapping equation 1 onto equation 3 for $FePS_3$ thus requires the exchanges and anisotropies in table I to be consolidated to produce an effective first-neighbour exchange, J^{eff}.

The parameter Δ^{cf}, representing the strength of the crystal field interactions, may not map directly onto the single ion term in table I, Δ. The mapping will depend on the degree by which the parameters in table I can be consolidated into J^{eff} and into converting $\mathbf{S} \rightarrow S^z$, with Δ^{cf} able to compensate for discrepancies.

Theory studies agree that the model will undergo a critical phase transition if Δ^{cf} and J have the same sign, or if $\Delta^{cf} = 0$. The transition is present at zero temperature, whereby it becomes a quantum phase transition. If they are of opposite sign, the phase transition can switch from critical to first-order at a tricritical point depending on the ratio Δ^{cf}/J^{eff}. The tricritical point appears in zero applied field for spin $S = 2$ on a honeycomb lattice at a ratio $\Delta^{cf}/J^{eff} \approx -1.495$, where it occurs at a reduced temperature of $k_B T/J^{eff} \approx 1.13$ [15, 23]. Tricritical points are found for decreasing ratios of $\left|\Delta^{cf}/J^{eff}\right|$ as a function of an increasing transverse field, H^x/J^{eff}, to $\Delta^{cf}/J^{eff} = -1.3466$, where the point appears at $T = 0$ and $H^x/J^{eff} = 0.9610$. The points are not found outside the range $-1.3466 \geq \Delta^{cf}/J^{eff} \geq -1.4971$ and $H^x/J^{eff} \leq 0.9610$ [15].

Rudimentary estimates for J^{eff} and Δ^{cf} may be made for $FePS_3$. The values in table I may be used to calculate $J^{eff} = \sum_i z_i J_i$ and to set $\Delta^{cf} = \Delta$, giving J^{eff} and Δ^{cf} to have the same sign for both sets of parameters in the table. Additionally, molecular field theory [24] can be applied to the anisotropic Curie-Weiss temperatures determined from the paramagnetic susceptibilities

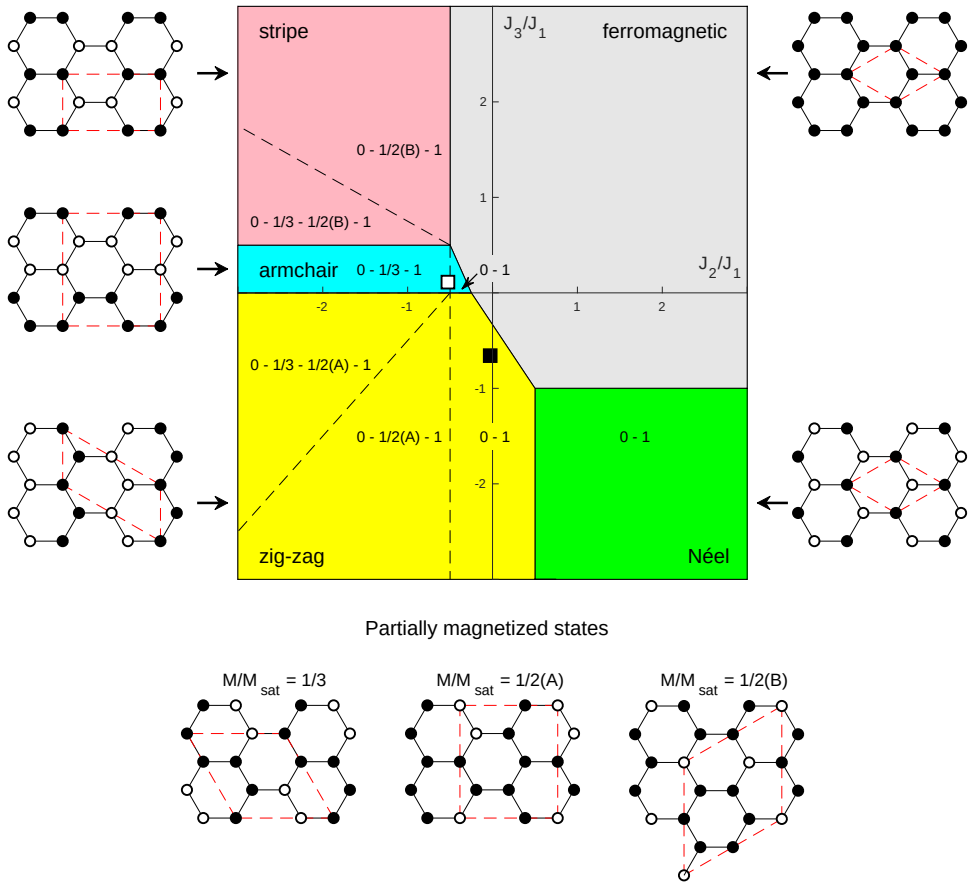


FIG. 2. Calculated phase diagram for the Ising Hamiltonian (equation 2) on a honeycomb lattice, along with the number and magnitude of plateaus present in the magnetisation for $\mathbf{H} \parallel \mathbf{c}^*$. The solid lines between the coloured regions mark the boundaries between the stable structures in zero field. The stable structures evolve into either partially or fully magnetized states with an increasing magnetic field, and the dashed lines demarcate the regions with different field evolutions. The establishment of each structure will create a plateau in the magnetization as the field is increased, and the magnitudes of the magnetization for each plateau are noted as the fraction of the saturation moment, M/M_{sat}, in the corresponding region of the phase diagram. Schematics for the different magnetic structures are shown, with open and filled circles representing the two directions for the spins, along with a representation of the unit cell for each bound by the red dotted lines. Note that there are two possible structures with $M/M_{sat} = 1/2$, labelled (A) and (B) respectively. The energies for all the states are given in Table II. Data points for the values in Table I are plotted on the figure as square symbols, with the values from Okuda *et al.* [19] are shown as a white-filled square and the values from Lançon *et al.* [11] shown as a black-filled square.

[14]. Again, this calculation gives J^{eff} and Δ^{cf} to have the same sign. The estimates suggest that $FePS_3$ should not have a tricritical point, and should have purely critical transitions to higher-field phases. However, a more sophisticated calculation, or an extension of the theory to include further neighbours on the honeycomb lattice, may show that a tricritical point is still possible.

III. EXPERIMENTS

Single crystal samples were made using a vapour transport method that has been previously described in detail [11]. Summarizing briefly, stoichiometric quantities of pure Fe, P, and S ($\geq$ 99.998%) were sealed in evacuated quartz tubes that were then placed in a horizontal two-zone furnace, with the elements placed in one of the two zones. Temperature gradients were applied between the zones. Initially, the gradient was 700°C:750°C with the elements in the cooler zone. This gradient was maintained for 12 days to allow the elements to react. The gradient was then inverted to 670°C:620°C for 21 days and plate-like $FePS_3$ crystals of dimensions $\sim 10 \times 10 \times 0.1\text{mm}^3$ formed in the cooler zone. The $\mathbf{c}^*$ was parallel to the normal of the platelets.

A single crystal was selected for the magnetisation measurements. $FePS_3$ is prone to crystal twinning from rotations of the $\mathbf{c}$ axis by 120° about the normal to the platelets [9]. The crystal quality and twin population were verified using the D10 neutron diffractometer at the Institut Laue-Langevin, Grenoble. The crystal was established to be very high quality with a domain popu-

TABLE II. The classical (mean-field) energies for the magnetic structures appearing in Figure 2.

Low-field structures	
Ferromagnetic	$-S^2\left(3J_1+6J_2+3J_3\right)/2+H^z$
Néel	$S^2\left(3J_1-6J_2+3J_3\right)/2$
Zig-zag	$S^2\left(-J_1+2J_2+3J_3\right)/2$
Armchair	$S^2\left(-J_1+2J_2+J_3\right)/2$
Stripe	$S^2\left(J_1+2J_2-3J_3\right)/2$
Partially-magnetised states	
$M/M_{sat}=1/3$	$S^2\left(-J_1+6J_2-J_3\right)/6+H^z/3$
$M/M_{sat}=1/2$ (A)	$-S^2J_1/2+H^z/2$
$M/M_{sat}=1/2$ (B)	$-3S^2J_3/2+H^z/2$

lation ratio of 0.89:0.09:0.02.

$FePS_3$ crystals are very soft and can be easily cleaved using a razor blade. Small parts of the crystal that had been aligned using neutron diffraction were cut for magnetisation measurements. The pieces were cut according to the known orientation of the parent crystal, and thus it was straight-forward to mount them in a magnetometer such that the magnetic field was applied along known crystallographic directions.

SQUID magnetometry up to 5 Tesla was performed using a MPMS magnetometer at the Institut Néel, Grenoble. No glue was used to mount the sample, and the same piece of crystal was used for all measurements. The sample was placed on a hemicylindrical quartz rod and then bound using plastic film before being placed in a plastic drinking straw for measurements with fields applied along the **a** and **b** axis. For fields along the $\mathbf{c}^*$ axis, the sample was sandwiched between two quartz cylinders and then the ensemble was placed in a plastic straw.

High field measurements were performed using the 65 Tesla pulsed magnets at the National High Magnetic Field Laboratory, Los Alamos. Figure 3 shows the time-dependence of a typical pulse to 65 Tesla. The pulse shape differs to that shown by Okuda *et al.* which was more symmetric [19]. Small parts of aligned crystal were placed in plastic capsules that had an inner diameter of ~ 0.6 mm and a length of ~ 5 mm. Some samples were fixed to wooden mounts to maintain their orientation, especially for the field applied along $\mathbf{c}^*$ axis. The sample orientations were fixed with a small amount of vacuum grease. Samples, photographed after the experiments, are shown in figure 4.

The samples were mounted in a magnetisation probe, which consisted of a pick-up coil with counter-wound compensation coils. Offsets for the compensation coils were adjusted to cancel the induction from the pulsed field, attempting to leave only the signal from the sample. The measurements were performed using the extraction technique, whereby a measurement with the sample in the centre of the pick-up coil would be followed by a measurement to the same maximum field with the sample outside the pick-up coil. The difference between the two measurements was taken to give the response of the sample.

Temperature control was achieved using a liquid helium cryostat. Temperatures below 4.2 K could be achieved with the samples in liquid or gaseous helium.

The probe measured the rate of change of the voltage in the pick-up coil, dV/dt. A correlated measurement in the compensation coil was converted to the rate of change of the induction, dB/dt via a calibrated constant specific to the probe. The data were recorded as a function of time with 1 MHz frequency. The field at a specific time was calculated by a discrete integration by time of dB/dt from the beginning of the pulse, while the corresponding magnetisation, in arbitrary units, was calculated by a similar integration over dV/dt.

A pulsed-field measurement is time-dependent, raising a question as to whether a sample is in thermal equilibrium at every point in time during the measurement. The efficiency of the connection with the thermal bath, and the rate that heat may be exchanged between the bath and the sample, dictate whether this is the case. Measurements below 4.2 K could be performed with the sample in liquid or gaseous helium. Liquid helium is a much better heat conductor than gas, and thus the sample has a much better connection to the thermal bath when it is in liquid. Measurements in liquid helium are thus more representative of being isothermal, while the measurements in gaseous helium are more representative of being adiabatic.

IV. RESULTS

Figure 5 shows the magnetisation measurements of $FePS_3$ for a field applied along different crystallographic directions. The data were measured at 4 K with the sample in gaseous helium.

The SQUID measurements show that the magnetisation is isotropic when the field is applied in the ab planes, increasing linearly with field up to the maximum of 5 Tesla. The magnetisation also increases when the field is applied normal to the ab planes, i.e. parallel to the $\mathbf{c}^*$ direction, but the rate of increase is substantially smaller. No phase transitions are observed, and the data are consistent with equation 1.

The pulsed field measurements with the field in the ab planes also show that the magnetisation increases linearly with field up to ~ 30 Tesla. These data could therefore

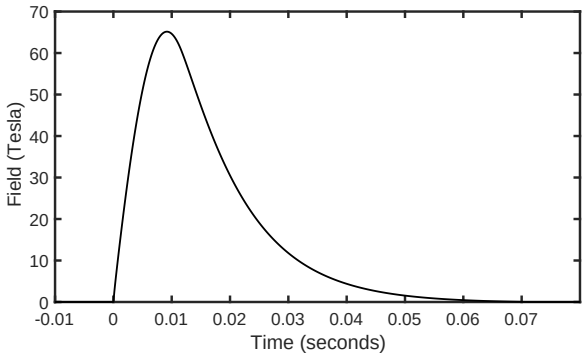


FIG. 3. The time-dependence of a typical pulse to 65 Tesla.

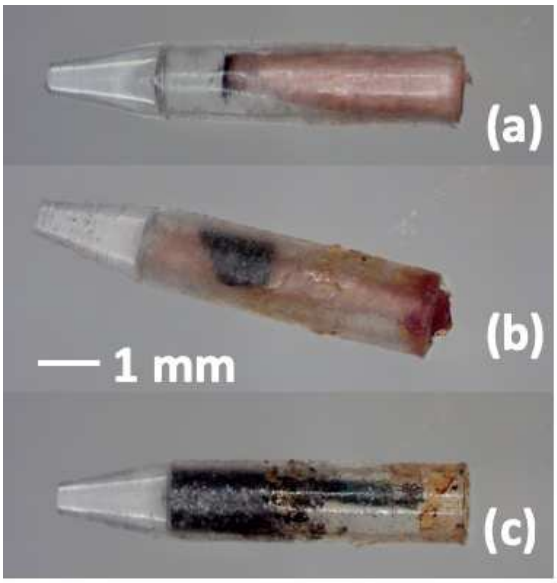


FIG. 4. Post-measurement photographs of the samples used for the pulsed field experiments for (a) **H** || **c***, (b) **H** || **a**, and (c) **H** || **b**. The $FePS_3$ samples are black, and have been inserted into plastic capsules. Samples (a) and (b) have been fixed to wooden mounts, whereas sample (c) was fixed directly to the wall of the capsule. A small amount of vacuum grease was used to fix the samples.

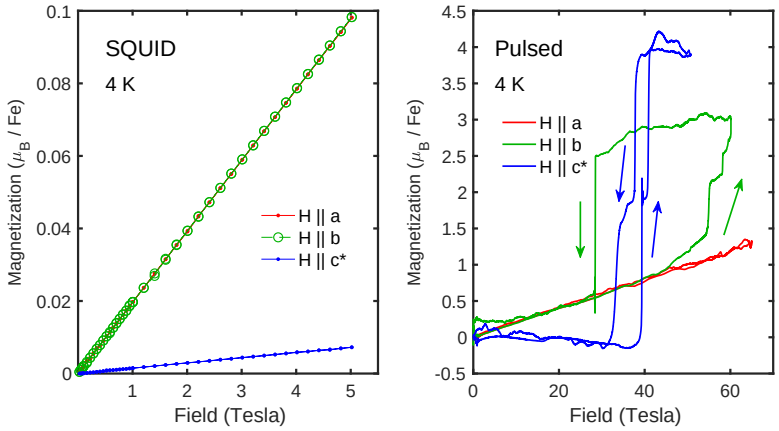


FIG. 5. SQUID and pulsed field magnetisation measurements of $FePS_3$ in gaseous helium, performed at 4 K for a field applied along different crystallographic axes. The arrows on the figure with the pulsed data show whether the field was increasing or decreasing for the corresponding data.

be converted into absolute units by comparing the gradients with those for the SQUID measurements. The same comparison could not be performed for the $\mathbf{H} \parallel \mathbf{c}^*$ data. These pulsed field measurements show the magnetisation to be essentially zero below ~ 30 Tesla, even becoming slightly negative due to a probable slight discrepancy between the sample-in and sample-out measurements. The $\mathbf{H} \parallel \mathbf{c}^*$ data were eventually expressed in absolute units by comparison with the pulsed-field $\mathbf{H} \parallel \mathbf{b}$ data, as will be explained below.

The $\mathbf{H} \parallel \mathbf{c}^*$ data are consistent with the previous measurements by Okuda *et al.* [19]. The data show essentially zero magnetisation with increasing field up to ~ 38 Tesla, at which point the magnetisation begins to increase before a discontinuous jump to 2 μ_B/Fe at 39.35 Tesla. The jump is so abrupt that ringing is observed in dV/dt causing an apparent spike in the magnetisation. A magnetisation plateau occurs within a field range of $39.35 \leq \mathrm{H} \leq 40.7$ Tesla before a second jump to 4 μ_B/Fe at 41.3 Tesla. The second jump is less rapid than the first. Measurements to 65 Tesla showed that no subsequent plateaux were observed to the maximum field. The two transitions are observed with decreasing field, however they are both less abrupt and they show hysteresis, occurring at lower fields of ~ 37.8 Tesla and ~ 33.8 Tesla. The data were reproducible and the sample, shown after the measurements in figure 4(a), was unaffected by the pulsed field.

The magnetisation for $\mathbf{H} \parallel \mathbf{a}$ continues to increase linearly with increasing field to the maximum 65 Tesla and decreases back to zero with no hysteresis. Again, the data were reproducible and the sample, shown in figure 4(b), was unaffected by the pulsed field.

For $\mathbf{H} \parallel \mathbf{b}$, however, the magnetisation becomes highly non-linear and is also highly hysteretic. The arrows on the figure show the direction of the changing field. The data are linear with increasing field to ~ 40 Tesla. The magnetisation then begins to increase more rapidly with increasing field before beginning an apparent cascade of discontinuous jumps to the maximum field. The sample was then locked into an apparent metastable state with an increased magnetisation. It maintained this state with decreasing field to 28.5 Tesla, where it underwent a discontinuous decrease in magnetisation to the same values as those for increasing field. Again, ringing was observed due to the abruptness of the transition giving rise to an apparent negative spike in the magnetisation.

The $\mathbf{H} \parallel \mathbf{b}$ data was used to express the $\mathbf{H} \parallel \mathbf{c}^*$ data in absolute units by assuming that that height of the discontinuous jump with decreasing field for the former data was equal in magnitude to the discontinuous jump to the first magnetisation plateau for the latter data. The calibration is prone to error as the $\mathbf{H} \parallel \mathbf{b}$ data do not saturate and there is no guarantee that the magnetisation would not continue to increase. However, the calibration appears to be reasonable in that the maximum magnetisation for the $\mathbf{H} \parallel \mathbf{c}^*$ data becomes 4 μ_B/Fe, which is acceptable for the saturation moment of the $S = 2$, Fe^{2+} ions.

The $\mathbf{H} \parallel \mathbf{b}$ data were qualitatively reproducible but showed quantitative differences with subsequent measurements. The source of the differences became apparent when the sample was removed from the instrument. Figure 4(c) shows the sample after the measurements. The sample was initially a single piece of crystal approximately 4 mm long. Part of the original sample can be seen inside the capsule to the right of the figure. The part of the sample in the centre of the field had suffered significant delamination, apparently due to substantial magnetostriction at high fields, coating the inside of the capsule with small crystallites. The inability to have quantitatively reproducible data was due to the deterioration of the sample from delamination successive pulses.

Measurements at 4.2 K showed profound differences depending on whether the sample was in liquid or gaseous helium, particularly when the field was applied along the $\mathbf{c}^*$ axis as shown in figure 6. These measurements were performed on the same sample, shown in figure 4(a). Both data sets show effectively zero magnetisation for increasing field below ~ 38 Tesla with an extremely abrupt transition. The transition was at a slightly higher field, $\mathrm{H} \sim 41.9$ Tesla, when the sample was in liquid helium. The sample in this environment did not show a second transition, however, maintaining a magnetisation plateau to the highest applied field of 65 Tesla.

The magnetisation plateau for the sample in liquid helium also showed substantially greater hysteresis than for the sample in gaseous helium. A transition to zero magnetisation is observed at 21.14 Tesla as the field decreased. The transition is equally as abrupt as the transition observed when the field was increasing.

Figure 6 also shows measurements performed for $\mathbf{H} \parallel [110]$. The [110] direction, shown in Figure 1(b), has a substantial vector component perpendicular to the ferromagnetic chains. Measurements in this orientation were reproducible and inspection at the end of the experiment showed that the sample suffered from minimal delamination and degradation. These measurements were thus particularly useful as they permitted a systematic study of the temperature- and field-dependence of the phase transitions observed when the field was applied along $\mathbf{b}$.

The data for the sample in gas are qualitatively similar to those for $\mathbf{H} \parallel \mathbf{b}$ in figure 5, with the major difference being a much smoother transition from one linear regime to a second linear regime as the field increased between 40 and 60 Tesla. The magnetisation is still highly hysteretic with an extremely abrupt transition back to the low-field magnetisation at 28.77 Tesla, corresponding to the same abrupt transition for $\mathbf{H} \parallel \mathbf{b}$, suggesting that the magnetic structure was locked into a similar metastable state. The magnetisation with increasing field looks identical for samples in gaseous or liquid helium, however the abrupt transition with decreasing field decreases in the latter case to 22.24 Tesla.

The high-field magnetisation was measured as a func-

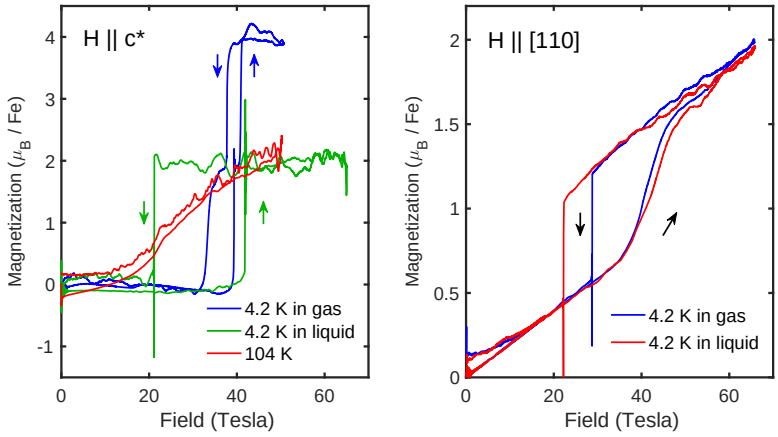


FIG. 6. High field magnetisation for the field applied along different crystallographic directions, and as a function of whether the sample was in a liquid or gaseous helium environment.

tion of temperature. Figure 6 shows a measurement at 104 K for $\mathbf{H} \parallel \mathbf{c}^*$. The data are very similar to those shown by Okuda *et al.* [19], with the data showing a smooth non-linear increase in magnetisation with increasing field and no notable hysteresis.

The temperature dependence for the magnetisation with $\mathbf{H} \parallel [110]$ is shown in figure 7. All the measurements were performed with the sample in gaseous helium. The data show that the magnetisation with increasing field is similar at all temperatures below 20 K. However, the abrupt transition with decreasing field is heavily dependent on temperature, appearing at increased fields with increasing temperature and disappearing between 11 and 12 K. The magnetisation also becomes less hysteretic at higher temperatures. Data at 20 K hint at a weak plateau at ~ 42 Tesla. Measurements at 100 K showed data that were qualitatively similar to those for $\mathbf{H} \parallel \mathbf{c}^*$.

The $\mathbf{H} \parallel [110]$ magnetisation was measured at 4.2 K as a function of the maximum field for the pulse, H_{max}. The data are shown in figure 8. The measurements were performed with the sample in liquid helium. The data show that the metastable state is only created for $H_{max} > 47$ Tesla. The abrupt transition with decreasing field is approximately independent of H_{max}, occurring at a smaller field than observed when the sample is in gaseous helium in a manner consistent with the data in figure 6.

V. DISCUSSION

The data suggest that $FePS_3$ at 4.2 K undergoes first-order phase transitions in fields above 40 Tesla. The conclusion is supported by the abruptness of the transitions and the hysteresis in the magnetisation shown in Figure 5, and by the differences between measurements performed in liquid or gaseous helium shown in Figure 6. These observations imply that a latent heat is involved in the transitions.

A. Field parallel to c*

The data for a sample in gaseous helium at 4.2 K with $\mathbf{H} \parallel \mathbf{c}^*$, given in Figure 5, show two transitions: one to $M/M_{sat} = 1/2$; and the second to $M/M_{sat} = 1$. The measurements confirm the experiments performed by Okuda *et al.* [19].

The second plateau for the same sample in liquid helium was not observed to the maximum applied field of 65 Tesla. A likely explanation is that isothermal $FePS_3$ at 4.2 K has a second transition to M_{sat} at fields higher than 65 Tesla, however this obviously could not be tested in the current experiment.

The discrepancies between the data and the exchange parameters in Table I can now be addressed. While the method used by Okuda *et al.* to estimate the field-dependence of the magnetisation was sound, they did not consider the stability of the magnetic structure in zero field and their values are incompatible with the observed magnetic structure for $FePS_3$. Arguably, there is some flexibility in their estimates. The exchange parameters were calculated from the magnitudes of the two critical fields at 4.2 K and the powder-average Curie-Weiss temperature. The hysteresis in the transitions is considerable, and the critical fields used for the calculation were averaged from the values on the pulse rise and fall. The paramagnetic susceptibility is highly anisotropic, and a broad distribution of values for Curie-Weiss temperatures have been previously published (c.f. [14]). The uncertainties in the data used by Okuda *et al.* allow for a considerable margin for error in their values for the exchange. It may be possible to find a solution that still gives reasonable estimates for the critical fields and Curie-Weiss temperature; for example changing the sign of J_3 would put the Okuda values on the region of the phase diagram in Figure 2 that is consistent with the observed high-field magnetisation.

However, the Okuda *et al.* parameters, or variations around them, do not give the spin wave dispersion ob-

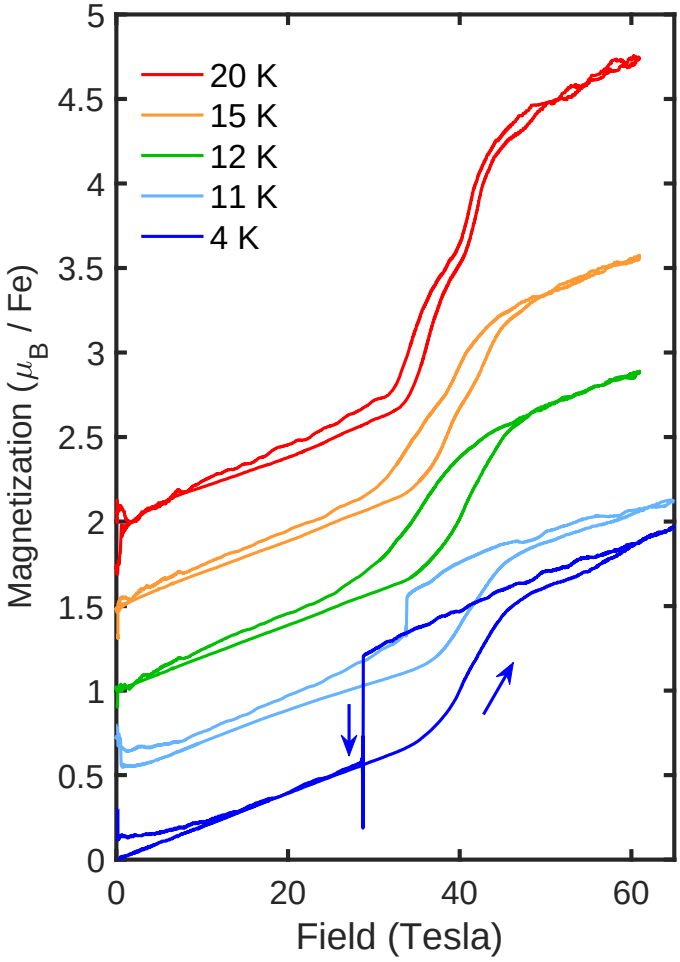


FIG. 7. High field magnetisation for **H** || [110] as a function of sample temperature. The data have been successively shifted up the vertical axis by 0.5 μ_B/ Fe for clarity. The sample was in a gaseous helium environment for all the measurements.

served in neutron spectroscopy. The values of Lançon *et al.* do, and they are consistent with the 'zig-zag' structure observed in zero field, but they do not give a transition to $M/M_{sat} = 1/2$ in Figure 2. In particular, the figure shows that this transition requires that $J_2 \leq -J_1/2$ while the unequivocal conclusion from spin wave analysis was that $J_2 \approx 0$.

Adapting the Hamiltonian in Equation 1 offers a possible solution to the contradiction. The Hamiltonian may be modified to allow for anisotropic exchange parameters in addition to a single-ion anisotropy, i.e.:

$$\begin{aligned}\hat{\mathcal{H}} = &-\sum_{\langle ij\rangle}\left(J_{ij}\left(S_i^x S_j^x + S_i^y S_j^y\right) + J_{ij}^{zz} S_i^z S_j^z\right) \\ &- \Delta\sum_i \left(S_i^z\right)^2 - H^z \sum_i S_i^z.\end{aligned} \tag{4}$$

The matrix form of Equation 4 is identical to that of Equation 1, as given by Lançon *et al.* [11]. The modification changes the elements along the matrix diagonal to:

$$\begin{aligned}&2J_2\cos(2\pi h) - \Delta - J_1 + 2J_2 + 3J_3 \\ \rightarrow\ &2J_2\cos(2\pi h) - \Delta - J_1^{zz} + 2J_2^{zz} + 3J_3^{zz}\end{aligned} \tag{5}$$

where the interlayer exchange is neglected and the reciprocal lattice corresponds to a magnetic unit cell defined in [11]. The modifications thus only affect those terms with no dependence on the reciprocal lattice vector, and Equations 1 and 4 will give identical dynamical structure factors so long as the sum of the non-**q**-dependent terms in Equation 5 are conserved, i.e. from the values in Table I:

$$-\Delta - J_1^{zz} + 2J_2^{zz} + 3J_3^{zz} = -7.08 \text{ meV} \tag{6}$$

The magnon dispersion from equation 4 is given by the values for J_{ij}, and these are equal to the values from Lançon *et al.* in Table I. Their value for Δ becomes meaningless as it is the sum in equation 6 which determines the magnon gap. The equation is underdefined and the individual parameters cannot be determined from the neutron data. However, the value of

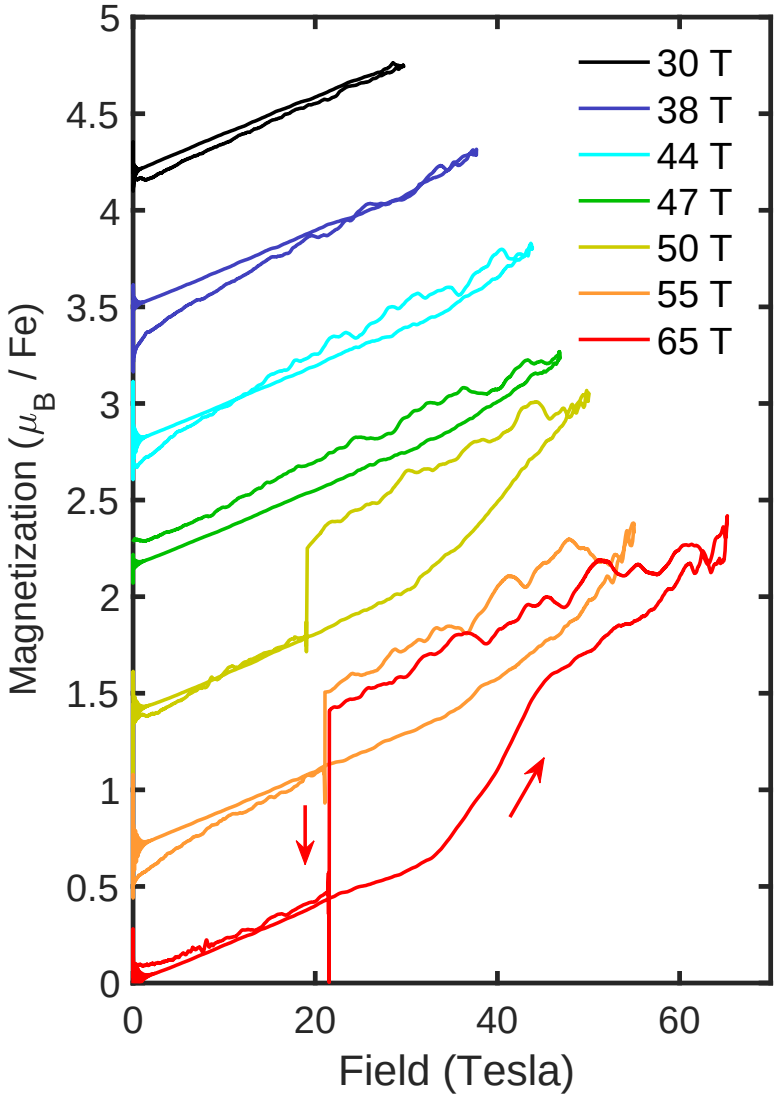


FIG. 8. High field magnetisation for **H** || [110] as a function of the maximum field for the pulse, H_{max}. The data have been successively shifted up the vertical axis by 0.7 μ_B/ Fe for clarity. The sample was at 4.2 K in a liquid helium environment.

$\Delta = 2.95$ meV given by Okuda *et al.* results from an independent measurement of the paramagnetic resonance on a Fe^{2+}-doped $CdPS_3$ crystal. This value may be substituted into equation 6 to produce an equality for the three values of J_{ij}^{zz}

The magnetic structure is determined by the classical energy which is given by the S^z terms in equation 4. The values for J_{ij}^{zz}, which do not need to be equal to the values for J_{ij}, may thus be compared directly with the stability phase diagram shown in Figure 2. If the value for J_2^{zz} were to become distinctly non-zero such that the conditions of $J_2^{zz} \leq -J_1^{zz}/2$ and $J_3^{zz} \leq J_2^{zz} + J_1^{zz}/2$ were satisfied, $FePS_3$ would be put in the correct part of the phase diagram for the observed high-field magnetisation in Figure 5. This would satisfy the observed behaviour of the magnetisation, which depends on the relative values of J_{ij}^{zz}, and the observed magnon dispersion, which depends on J_{ij} and the equality in equation 6, thus reconciling the contradiction.

B. Field perpendicular to c*

As shown in Figure 5, the high-field magnetisation for **H** || **a** shows no sign of any transition to 65 Tesla and suggests a gradual rotation of the magnetic moment along the **a** axis. The result is consistent with a critical phase transition to an eventual aligned paramagnetic state at a very large critical field, in a similar manner to that observed for the transition from a spin-flop phase to an aligned paramagnetic phase.

When **H** || **b**, however, the data suggest that a series of abrupt first-order transitions to metastable states occur in fields above 50 Tesla. The highest-field state appears to have 2 μ_B/Fe parallel to the **b** axis, as shown by the height of the abrupt transition observed as the field was

decreasing.

All of the Hamiltonians in equation 1−4 result in a magnetisation that is independent of the direction of a transverse field with respect to the crystal orientation. Further modifications are necessary to explain the difference between the high-field magnetisation for fields parallel to **a** and **b** in Figure 5. Two possible modifications may be proposed.

The first proposal involves the inclusion of extra anisotropy terms in addition to, or to replace, the single-ion anisotropy. It is tempting to include a Dzyaloshinski-Moriya term, or to further modify the anisotropic exchange in a manner similar to the Kitaev-Heisenberg model. The latter is particularly appealing as the 'zig-zag' antiferromagnetic structure is also found in compounds that are considered to be Kitaev-Heisenberg systems, such as Na_2IrO_3 [25] and α-$RuCl_3$ [26]. The extra anisotropy would introduce in-plane terms into the Hamiltonian which could give the directional dependence of the high-field magnetisation. However, it seems highly unlikely that these terms are sufficiently large to make a difference. The ordered moment direction is constrained to be normal to the planes by a strong uniaxial anisotropy, and there is no apparent chirality associated with the magnetism as, due to its $\mathbf{S}_i \times \mathbf{S}_j$ form, might result from an important Dzyaloshinski-Moriya anisotropy. The Néel temperature is large and the spin waves are well-defined in energy with no liquid-like continuum in the magnetic excitations, as might be expected for a Kitaev-Heisenberg model.

The second modification involves the inclusion of terms that couple the magnetic and crystal lattices. This is far more likely. The onset of antiferromagnetic order in zero field creates a discontinuity in the rate of change of the lattice parameters with respect to temperature, although the crystal space group does not change [8, 9], establishing that $FePS_3$ hosts significant magnetostriction. The violent delamination of a sample subjected to high fields with $\mathbf{H} \parallel \mathbf{b}$, as shown in Figure 4 implies that the magnetostriction places a considerable strain on the lattice in this orientation, possibly leading to a new crystal structure. The energies for forming new crystal structures, especially if they involve a relative movement of the ab planes, are relatively low due to the weak binding of the planes through van der Waals forces. It is tempting to support the hypothesis by inspecting the magnetic structure. The nearest-neighbour exchange is ferromagnetic. The ferromagnetic 'zig-zag' chains run along the **a** axis, while the moments are antiferromagnetically coupled along the **b** axis. A magnetocrystalline coupling may create significant frustration when the field is aligned along **b**. Furthermore, recent high-pressure studies of the crystal structure show that $FePS_3$ undergoes structural phase transitions from 4 GPa that amount to a shear of the planes along the **a** axis [27, 28], suggesting that motion along the **b** axis is energetically less favourable and potentially more prone to magnetostriction.

There are insufficient data to quantify any coupling between the magnetism and the crystal lattice, and any attempt to modify the Hamiltonian to include the coupling is beyond the scope of the current article . Probing the degree of coupling is experimentally difficult, as magnetic fields in excess of 50 Tesla are required to drive the transitions. The possibility to perform measurements of the specific heat and of crystal distortion due to magnetostriction will be explored in the future.

Final consideration may be paid as to whether $FePS_3$ might have a tricritical point, defined by the point where a first-order phase transition becomes a critical phase transition. The data in Figure 7 suggest that the transitions for $\mathbf{H} \perp \mathbf{c}^*$ are of first order for the lowest temperatures. However, the abrupt transition disappears above 11 K and the hysteresis disappears above 15 K, suggesting that transitions at higher temperature are more indicative of critical phase transitions. This is the predicted behaviour in the presence of a tricritical point [15, 17], thus it may be that such a point is present in $FePS_3$. The conjecture cannot be verified without a better understanding of the exact nature of the phase transitions and the Hamiltonian, including possible coupling of the magnetisation to the crystal lattice.

VI. CONCLUSIONS

Magnetisation measurements to 65 Tesla on $FePS_3$ at 4 K show first order phase transitions to ordered phases. The two transitions observed when the field is applied along $\mathbf{c}^*$ are not consistent with the exchange parameters derived from the spin wave dispersion, but can be predicted if anisotropic exchange parameters are introduced into the Hamiltonian. The magnetisation with $\mathbf{H} \perp \mathbf{c}^*$ is anisotropic, which cannot be understood from a simple magnetic Hamiltonian with a single-ion anisotropy. It is highly likely that some coupling between the magnetic and crystalline lattice must be included into the Hamiltonian to understand the results.

ACKNOWLEDGMENTS

The high-magnetic field measurements were supported by the US Department of Energy BES Science at 100T grant. The National High Magnetic Field Laboratory - Pulsed-Field-Facility is funded by the National Science Foundation Cooperative Agreement Number DMR-1157490 and DMR-1644779, the State of Florida and the U.S. Department of Energy. The authors gratefully acknowledge the support of the Institut Néel, Grenoble, for the SQUID measurements, and of the Institut Laue-Langevin, Grenoble, for the use of the D10 instrument.

[1] R. Brec, Solid State Ionics **22**, 3 (1986).
[2] G. Ouvrard, R. Brec, and J. Rouxel, Mater. Res. Bull. **20**, 1181 (1985).
[3] V. Grasso and L. Silipigni, Riv. Nuovo Cimento **25**, 1 (2002).
[4] J. G. Park, J. Phys.: Condens. Matter **28**, 301001 (2016).
[5] M. A. Susner, M. Chyasnavichyus, M. A. McGuire, P. Ganesh, and P. Maksymovych, Advanced Materials **29**, 1602852 (2017).
[6] F. Wang, T. A. Shifa, P. Yu, P. He, Y. Liu, F. Wang, Z. Wang, X. Zhan, X. Lou, F. Xia, and J. He, Advanced Functional Materials **28**, 1802151 (2018).
[7] J.-U. Lee, S. Lee, J. H. Ryoo, S. Kang, T. Y. Kim, P. Kim, C.-H. Park, J.-G. Park, and H. Cheong, Nano Letters **16**, 7433 (2016).
[8] P. Jernberg, S. Bjarman, and R. Wäppling, J. Magn. Magn. Mater. **46**, 178 (1984).
[9] C. Murayama, M. Okabe, D. Urushihara, T. Asaka, K. Fukuda, M. Isobe, K. Yamamoto, and Y. Matsushita, J. Appl. Phys. **120**, 142114 (2016).
[10] K. Kurosawa, S. Saito, and Y. Yamaguchi, J. Phys. Soc. Japan **52**, 3919 (1983).
[11] D. Lançon, H. C. Walker, E. Ressouche, B. Ouladdiaf, K. C. Rule, G. J. McIntyre, T. J. Hicks, H. M. Rønnow, and A. R. Wildes, Phys. Rev. B **94**, 214407 (2016).
[12] K. C. Rule, G. J. McIntyre, S. J. Kennedy, and T. J. Hicks, Phys. Rev. B **76**, 134402 (2007).
[13] K. Momma and F. Izumi, J. Appl. Crystallogr. **44**, 1272 (2011).
[14] P. A. Joy and S. Vasudevan, Phys. Rev. B **46**, 5425 (1992).
[15] W. Jiang, G.-Z. Wie, and Z.-H. Xin, physica status solidi (b) **225**, 215 (2001).
[16] O. Canko, E. Albayrak, and M. Keskin, Journal of Magnetism and Magnetic Materials **294**, 63 (2005).
[17] G. Wei, H. Miao, J. Liu, and A. Du, Journal of Magnetism and Magnetic Materials **320**, 1151 (2008).
[18] J. Strečka and M. Jaščur, Acta Phys. Slovaca **65**, 235 (2015).
[19] K. Okuda, K. Kurosawa, and S. Saito, in *High Field Magnetism*, edited by M. Date (North Holland, Amsterdam, 1983).
[20] T. Kudō and S. Katsura, Progress of Theoretical Physics **56**, 435 (1976).
[21] M. V. Gvozdikova, T. Ziman, and M. E. Zhitomirsky, Phys. Rev. B **94**, 020406(R) (2016).
[22] E. Rastelli, A. Tassi, and L. Reatto, Physica B **97**, 1 (1979).
[23] T. Kaneyoshi, J. W. Tucker, and M. Jaščur, Physica A: Statistical Mechanics and its Applications **186**, 495 (1992).
[24] D. C. Johnston, Phys. Rev. B **95**, 094421 (2017).
[25] S. K. Choi, R. Coldea, A. N. Kolmogorov, T. Lancaster, I. I. Mazin, S. J. Blundell, P. G. Radaelli, Y. Singh, P. Gegenwart, K. R. Choi, S. W. Cheong, P. J. Baker, C. Stock, and J. Taylor, Phys. Rev. Lett. **108**, 127204 (2012).
[26] A. Banerjee, C. A. Bridges, J.-Q. Yan, A. A. Aczel, L. Li, M. B. Stone, G. E. Granroth, M. D. Lumsden, Y. Yiu, J. Knolle, S. Bhattacharjee, D. L. Kovrizhin, L. R. Moessner, D. A. Tennant, D. G. Mandrus, and S. E. Nagler, Nature Mater. **15**, 733 (2016).
[27] C. R. S. Haines, M. J. Coak, A. R. Wildes, G. I. Lampronti, C. Liu, P. Nahai-Williamson, H. Hamidov, D. Daisenberger, and S. S. Saxena, Phys. Rev. Lett. **121**, 266801 (2018).
[28] Y. Wang, J. Ying, Z. Zhou, J. Sun, T. Wen, Y. Zhou, N. Li, Q. Zhang, F. Han, Y. Xiao, P. Chow, W. Yang, V. V. Struzhin, Y. Zhao, and H.-K. Mao, Nature Comm. **9**, 1914 (2018).